Mechanical characterization of bioprinted *in vitro* soft tissue models

2013 Biofabrication 5 045010

(http://iopscience.iop.org/1758-5090/5/4/045010)

Biofabrication **5** (2013) 045010 (10pp) doi:10.1088/1758-5082/5/4/045010

Mechanical characterization of bioprinted *in vitro* soft tissue models

Ting Zhang[1,2,3,7], **Karen Chang Yan**[4], **Liliang Ouyang**[1,2,3] **and Wei Sun**[1,2,3,5,6]

[1] Department of Mechanical Engineering, Biomanufacturing Engineering Research Institute, Tsinghua University, Beijing 100084, People's Republic of China
[2] Key Laboratory for Advanced Materials Processing Technology, Ministry of Education, Beijing 100084, People's Republic of China
[3] Biomanufacturing and Rapid Forming Technology Key Laboratory of Beijing, Beijing 100084, People's Republic of China
[4] Department of Mechanical Engineering, The College of New Jersey, Ewing, NJ 08628, USA
[5] Biomanufacturing Engineering Research Laboratory, Graduate School at Shenzhen, Tsinghua University, Shenzhen 518055, People's Republic of China
[6] Department of Mechanical Engineering, Drexel University, Philadelphia, PA 19104, USA

E-mail: t-zhang@mail.tsinghua.edu.cn

Received 24 June 2013
Accepted for publication 3 October 2013
Published 26 November 2013
Online at stacks.iop.org/BF/5/045010

Abstract

Recent development in bioprinting technology enables the fabrication of complex, precisely controlled cell-encapsulated tissue constructs. Bioprinted tissue constructs have potential in both therapeutic applications and nontherapeutic applications such as drug discovery and screening, disease modelling and basic biological studies such as *in vitro* tissue modelling. The mechanical properties of bioprinted *in vitro* tissue models play an important role in mimicking *in vivo* the mechanochemical microenvironment. In this study, we have constructed three-dimensional *in vitro* soft tissue models with varying structure and porosity based on the 3D cell-assembly technique. Gelatin/alginate hybrid materials were used as the matrix material and cells were embedded. The mechanical properties of these models were assessed via compression tests at various culture times, and applicability of three material constitutive models was examined for fitting the experimental data. An assessment of cell bioactivity in these models was also carried out. The results show that the mechanical properties can be improved through structure design, and the compression modulus and strength decrease with respect to time during the first week of culture. In addition, the experimental data fit well with the Ogden model and experiential function. These results provide a foundation to further study the mechanical properties, structural and combined effects in the design and the fabrication of *in vitro* soft tissue models.

(Some figures may appear in colour only in the online journal)

1. Introduction

Advancements in the field of tissue science and engineering have led to not only to a myriad applications in regenerative medicine, but also nontherapeutic applications such as drug discovery and toxicology screening, tissue-based sensors and tissue-based factories (Tissue Eng 2007). Current strategies to fabricate engineered tissue, especially engineered soft tissue, include the scaffold-based approach and the cell-encapsulated approach (Giordano *et al* 2009). While the use of these approaches has led to great success (Atala *et al* 2006, Lazic and Falanga 2011, McAllister *et al* 2009), it has been well-established that the matrix's material composition (Russo *et al* 2010, De Santis *et al* 2011), physicochemical properties

[7] Author to whom any correspondence should be addressed.

(Domingos *et al* 2012, Gloria *et al* 2012a), internal architecture (Gloria *et al* 2012b) and methods for its fabrication (Drury and Mooney 2003, Lutolf and Hubbell 2005, Hollister 2005) influence cellular behaviours (Kuo and Ma 2001, Yang *et al* 2001, Derby 2012) and the mechanism should be further studied.

Recent developments have been achieved by a series of bioprinting techniques that enable fabrication of complex, precisely controlled cell-encapsulated tissue constructs, through the mixing of cells with matrix materials and delivering of the mix automatically using computer-aided systems (Jakab *et al* 2008, Norotte *et al* 2009). These enabling bioprinting systems include laser-guided direct writing (Barron *et al* 2004), micropatterning (Lee *et al* 2008), 3D photopatterning (Liu and Bhatia 2002), multi-nozzle direct disposition (Khalil *et al* 2005) and inkjet printing (Mironov *et al* 2003). Several recent efforts have also demonstrated potential uses of bioprinted soft tissue constructs in therapeutic applications such as skin wound grafts (Lee *et al* 2009), osteochondral grafts (Fedorovich *et al* 2012) and vascular grafts (Khatiwala *et al* 2012), and nontherapeutic applications such as examining *in vitro* drug metabolism and pharmacokinetics (Chang *et al* 2008, 2010) and mimicking early morphogenesis (Jakab *et al* 2008).

An important aspect in the development of bioprinted soft tissue constructs/models is to mimic the complex structure of the matrix, cells and bioactive factors inside native tissue from both a spatial and a temporal perspective. Mimicking the *in vivo* mechanochemical microenvironment is one of the key issues in addition to selecting suitable biomaterials, optimizing the configuration of tissue constructs and fabrication methods (Lutolf and Hubbell 2005, Rehfeldt *et al* 2007, Vunjak-Novakovic *et al* 1999). In particular, it is known that the ECM formation takes time; therefore, it is critical to have a clear understanding of the mechanical properties and structural integrity of bioprinted soft tissue constructs under culture conditions before matrix formation by the cells takes effect. There are a few recent studies on characterizing the initial mechanical properties of soft tissue constructs after printing (Yan *et al* 2010, Fedorovich *et al* 2012). However, it is unclear how the mechanical properties and structural integrity of these constructs change with respect to time in the culture conditions.

The objective of this research is to examine the mechanical properties and structural integrity of cell-embedded gelatin/alginate soft tissue models, especially during the first week of culture. In this study, we have employed the 3D cell-assembly technique (Yan *et al* 2005) and constructed 3D *in vitro* soft tissue models with varying structures and porosities using the gelatin/alginate hybrid materials. Compression tests were conducted to characterize the mechanical properties of samples at day 0, day 1, day 3 and day 6. Compression moduli and yield strength were determined from the experimental data. Changes in mechanical properties and structural integrity were observed during the first week of culture. The effects of structural configuration on the initial mechanical properties were also investigated. Three nonlinear elastic material models (Fung 1993, Humphrey 2003, Gasser *et al* 2006) were employed to fit the experimental data; their applicability was also compared. In addition, assessment of cell viability and proliferation in these models was also carried out.

2. Materials and methods

2.1. Bioprinting system

The cell assembler consists of four modules, namely, the nozzle driving unit, the forming platform, the refrigeration module and the PMAC numerical control (NC) system. Figure 1 shows a picture of the actual machine and a schematic of the system. The two-nozzle system allows for filling two different materials/cells and forming gradient-materials/cell structures. The nozzle system is controlled by the PMAC NC system. By combining the 3D motion unit, constructs with mixed materials/cells can be printed based on the CAD model. A refrigeration module is integrated into the system to form a low-temperature chamber, which can aid the crosslinking of biomaterials. For instance, a temperature of 3–10 °C is appropriate for the physical crosslinking of gelatin-based materials (Yan *et al* 2005, Liu *et al* 2011).

2.2. Matrix material selection

One of the key considerations for selecting matrix material is to imitate the structure and function of the natural extracellular matrix (ECM) (Drury and Mooney 2003, Subramanian *et al* 2009). Comparing with synthetic degradable polymers, natural polymers are more similar to natural ECM in terms of chemical composition, hydrophilicity and stiffness. Furthermore, multiple materials are often applied in practice to circumvent the limitation of a single polymer's physicochemical properties. Here we chose gelatin and alginate as the matrix materials for 3D soft tissue models (Yan *et al* 2005). Gelatin is a peptide polymer hydrolyzed from collagen, which performs well in terms of cellular affinity but has weak mechanical properties (Awad *et al* 2004). Both physical and chemical crosslinking are suitable for gelatin. Alginate, a polysaccharide carbohydrate extracted from alga, is similar to the glycosaminoglycan (GAG) in natural ECM. Alginate hydrogel can be acquired from chemical crosslinking with Ca^{2+} and other bivalent cations, which can strengthen the structural stability of the model. A two-step crosslinking process (physical and chemical) is employed before we culture the printed gelatin/alginate structures at 37 °C (Yan *et al* 2005, Liu *et al* 2011).

2.3. Structure design

Cell assembler can produce a variety of 3D structures ranging from cube, cylinder and tube to some complex user-defined 3D structures. Figure 2 illustrates an example of 3D soft tissue models with 0°/90° layout configuration. The presence of voids allows for transporting nutrients and metabolites. Clearly, design parameters of the structure such as filament diameters and gaps between two adjacent filaments affect the porosity of printed constructs. Assuming filaments are uniform cylinders, the porosity of printed constructs, p, can be estimated using (1)

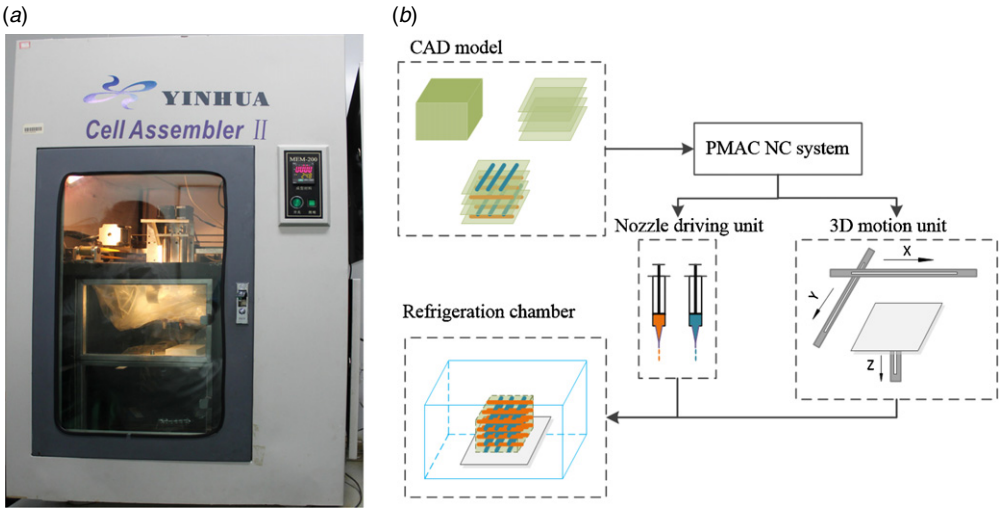

Figure 1. (*a*) The cell assembler and (*b*) a schematic of the system.

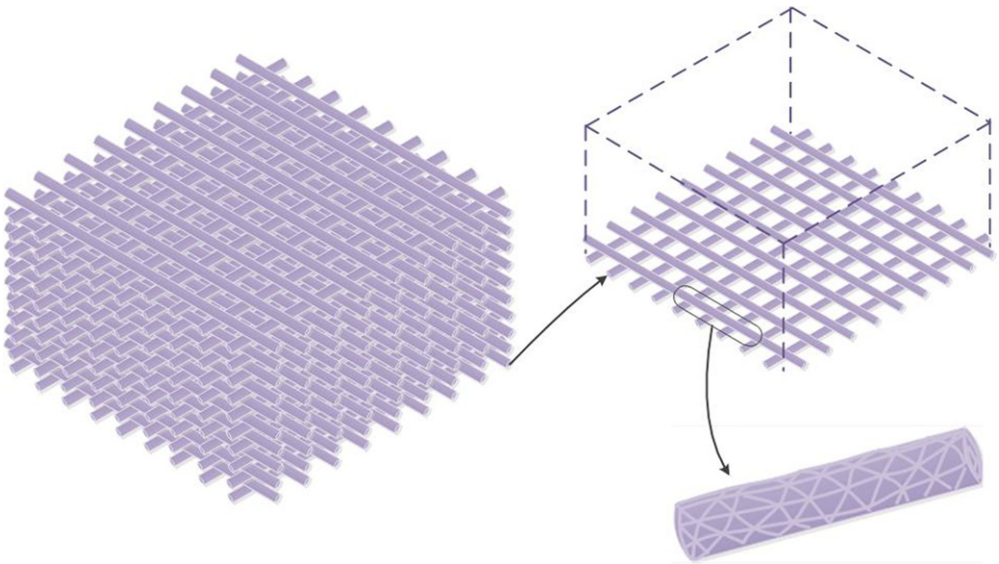

Figure 2. Example structure of printed soft tissue models with 0°/90° configuration.

$$p = 1 - \frac{\frac{1}{4}\pi d^2 \cdot \left(\frac{L}{t_x} - 1\right) L \cdot n}{L^2 \cdot nt'} = 1 - \frac{\pi d^2}{4t'L}\left(\frac{L}{t_x} - 1\right) \quad (1)$$

where d and L are the filament diameter and the side length of a cubic model, respectively. t_x is the filament gap, n is the number of layers and t' represents the gap between layers. 0.15 mm was used for t' in this study.

A trial in varying the filament gap from 0.7 to 1.2 mm was conducted; a filament gap of 1.0 mm yielded the best results considering the stability and functionality of the printed structures. In addition to 0°/90° configurations (90° structure), configurations with 0°/60°/90° layers (60° structure) were added to clarify the structural influence, which was designed to form a series of equilateral triangle units viewed from above with an angle of 60° between two adjacent layers.

2.4. Material preparation and the bioprinting process

The gelatin (Type B, Sigma Chemical) solution and the alginate (Sigma Chemical) solution were both prepared with double-distilled water. The solution concentrations were 20% (w/v) for gelatin and 7.5% (w/v) for alginate, respectively. The cells used in soft tissue models were C2C12 mouse myoblasts. This cell type is considered as the prime choice for studying proliferation and differentiation of myoblasts. It is also known that C2C12 is sensitive to loading stimulation (Ceelen *et al* 2009). Cells were made into cell suspension at a concentration of 6×10^6 cells ml^{-1}. The cell suspension was then mixed with the alginate and gelatin solutions at the ratio of 1:2:3. All material preparation was conducted in the ultra-clean bench. Once mixed, the printing materials were stirred and put in a 37 °C incubator for 10 min in order to achieve uniformity of materials.

Printing process parameters for fabricating the soft tissue models were set at a scanning speed of 7 mm s^{-1}, a jet speed of 0.01 mm s^{-1} and an interlayer distance of 0.15 mm. A nozzle with a diameter of 150 μm was used. Physical crosslinking was achieved in the refrigeration chamber at 3–4 °C. It took ~15–20 min to fabricate a model of 30 layers with the side length of 10 mm. Once formed, the samples

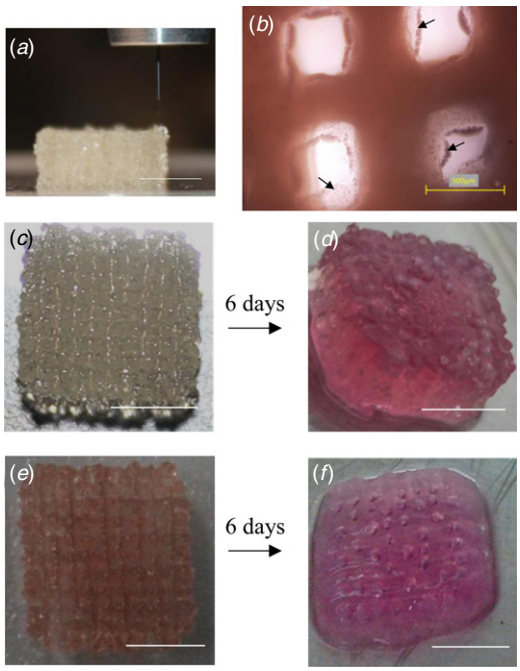

Figure 3. (*a*) The sample thickness is 5 mm. Reverse crosslinking of gelatin was observed; (*b*) separation of gelatin (indicated by black arrows) along the boundary of macro voids after 10 h culture. The appearance of acellular constructs (*c*) and (*d*) and cellular models (*e*) and (*f*) after culture for six days. Scale bar for (*a*) and (*c*)–(*f*) is 5 mm.

were immersed in the 5% (w/v) $CaCl_2$ solution for 2 min. After washing with PBS, the samples were placed into an incubator at 37 °C and 5% CO_2. The culture medium used was high glucose DMEM (GIBCO, Invitrogen Corporation, USA) supplemented with 100 unites ml^{-1} penicillin (Solarbio, China), 100 unites ml^{-1} streptomycin (Solarbio, China) and 10% FBS (Hyclone). The medium was changed every other day.

2.5. Live/dead staining and cell proliferation

To test cell viability, the printed structures were then immersed in 1 μmol ml^{-1} calcein acetoxymethylester (calcein-AM) and 2 μmol ml^{-1} propidium iodide (PI) for 15 min to stain live cells (green) and dead cells (red), respectively, when visualized using laser confocal microscopy (LSM710META, Zeiss). The structures were washed three times with PBS before and after live/dead staining. The count/size tool of Image-Pro Plus was used to determine the quantity of live/dead cells. For calculating cell viability, three samples were used and fluorescent images were taken at different locations for each sample.

To test cell proliferation, the printed structures were firstly immersed in 55 μg ml^{-1} sodium citrate and placed inside an incubator at 37 °C for 10 min to dissolve the structures and get homogeneous cell suspension. 100 μl cell suspension and 10 μl Cell Counting Kit-8 (CCK-8, DOJINDO) were added in each well of the 96-well plate. The blank control followed the same protocol, using the acellular constructs. The plate was put into a microplate reader (BIO-RAD, Model 680) after incubation for 2 h at 37 °C. The average optical density (OD) value was calculated by subtracting the blank control value.

2.6. Compression test and mechanical data processing

The EnduraTEC ELF 3200 (BOSE), a dynamic mechanical testing system, was used to test the compression properties of the formed soft tissue models. Both the ±450 N and ±250 g force sensors were used in our study. Unconstrained uniaxial compression tests were conducted with a loading rate of 0.05 mm s^{-1}, and the data acquisition rate of 20 points s^{-1} was set up.

The load-displacement curve were obtained from compression tests; the corresponding stress–strain curve can be determined based on (2) and (3) (Masouros *et al* 2009):

$$\sigma = \frac{F}{S} = \frac{F}{ab} \tag{2}$$

$$\varepsilon = \frac{\Delta h}{h_0} \tag{3}$$

where a, b and h_0 are the length, width and initial height of the sample respectively. Three samples were prepared for each test parameter. Due to slight differences in the sample sizes, linear interpolation was used to calculate the average stress data, ensuring all the data points share the same strain arrangement.

Fung's quasi-linear viscoelastic (QLV) theory provides meaningful phenomenological fit coefficients and is widely applied to many biological soft tissues (Pai and Ledoux 2011). The QLV theory assumes the elastic and time-dependent properties are separable and uses a linear combination of these nonlinear terms to describe the resultant stress.

In this study, we have focused on the elastic behaviour of the 3D *in vitro* soft tissue model. Hence, the elastic function is considered here. Exponential function and power function are widely used as given by (4) and (5) respectively (Pai and Ledoux 2011, Nekouzadeh *et al* 2007),

$$\sigma = A(e^{B\varepsilon} - 1) \tag{4}$$

$$\sigma = A\varepsilon^B. \tag{5}$$

Due to the nonlinear behaviour of the soft tissue model, the Ogden hyperelastic model is also considered to fit the stress–strain data. Deduced from the Ogden strain energy formula, the final stress expression is given by (7) (Umale *et al* 2011)

$$\sigma = \sum_{k=1}^{n} \mu_k (\lambda^{\alpha_k} - \lambda^{\frac{-\alpha_k}{2}}) \tag{6}$$

where μ_k is the partial tensor modulus, α_k is the index of partial tensor part and λ is the axial stretch ratio. As for compression tests, λ is the compression ratio and is equal to h/h_0 and $\sigma = F/ab$ is negative for compression. Stress data was reversed to be positive to achieve a typical stress–strain curve. When $n = 1$, the final fitting function is changed as shown below,

$$\sigma = \mu((1+\varepsilon)^{\alpha} - (1+\varepsilon)^{-\frac{\alpha}{2}}). \tag{7}$$

3. Results

3.1. Morphology and structural integrity of printed samples

3D structures with length of 10 mm, width of 10 mm and height of 5.0 mm were printed (figure 3(*a*)). Two groups of

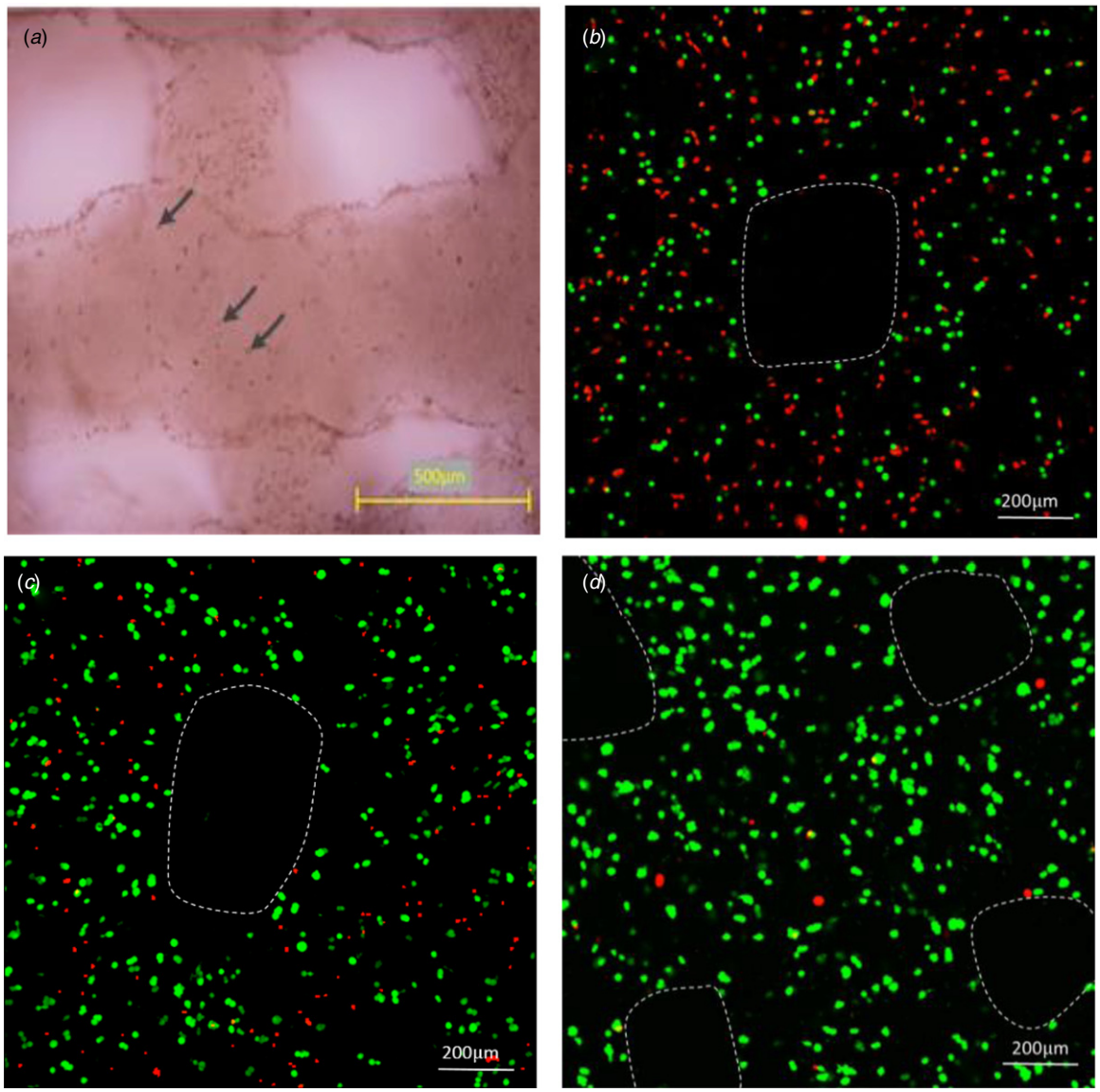

Figure 4. Micrograph of cell distribution and laser confocal imaging of viability staining. (*a*) Cells distribute uniformly in the models, indicated by black arrows. (*b*)–(*d*) Cells labelled with calcein-AM and PI within 3D structures were imaged with a laser confocal microscope. Live and dead cells were fluorescent green and fluorescent red, respectively. The macro voids are indicated by white dashes. (*b*) At day 0, (*c*) at day 1 and (*d*) at day 2.

samples were printed (figures 3): (*c*) and (*d*) were the acellular constructs; *e* and *f* were the soft tissue models with cells. The structural integrity of both groups was also observed from day 0 to day 6 (see figures 3(*c*)–(*f*)). As the culture time increases, it is seen that 3D acellular constructs (*c*) and (*d*) maintain good structural integrity with no obvious collapse. However, 3D soft tissue model samples (*e*) and (*f*) show decreasing structural integrity. In particular, matrix materials degrade away significantly and morphological features also become unclear after six days.

It is noted that the gelatin material within the samples was crosslinked at low temperature, therefore, when cultured at 37 °C, gelatin gel translated into solution as a consequence of reverse crosslinking. Figure 3(*b*) shows the separation of gelatin around the boundary of macro voids.

3.2. Cell viability and proliferation

Cells in the soft tissue models were surrounded by matrix materials as seen in figure 4(*a*). Figure 4(*b*) displays a fluorescent image of the Calcein–AM/PI stained sample with live cells (green) and dead cells (red). Based on image analysis, the average viability of cells in structures was 54.72% within 2 h after printing (see figure 4(*b*)). This value increased greatly after 24 h (see figure 4(*c*)) and very few dead cells were observed after two days (see figure 4(*d*)). The histogram of cell proliferation using CCK-8 is also shown in figure 5, indicating an increasing trend during the first four days and a decreasing trend from day 4 to day 5. This suggests that a proliferation saturation point was reached at day 4.

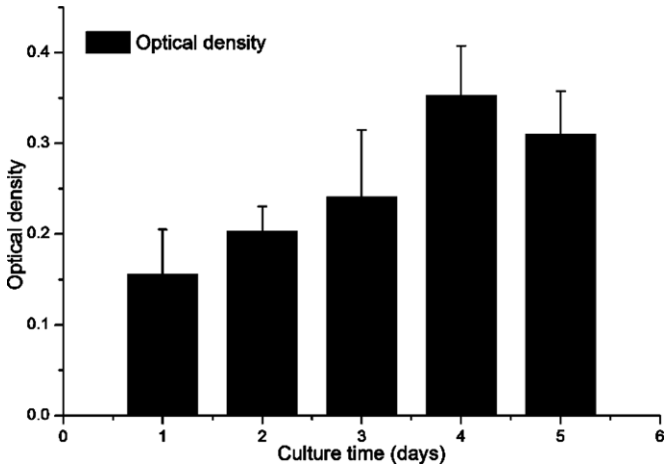

Figure 5. Cell proliferation from day 1 to day 5.

3.3. Mechanical characterization

3.3.1. Effects of culture time and cells. Figure 6 plots the nonlinear stress–strain curves of acellular constructs at day 0 and soft tissue model samples at day 0, day 1, day 3 and day 6. It is shown that the results of the acellular constructs yielded higher compression modulus in the high strain region and much higher yield strength. It is also seen that the strength of the soft tissue model decreases drastically after 1 day of culture, and the stress level becomes very small after three days of culture. From close-up, the stress–strain curves at day 3 and day 6 follow the same trend.

3.3.2. Effects of structural configuration. For the model with 0°/90° configuration, different filament gaps mean different porosity, and porosity is a significant factor for the mechanical properties of porous structures. Here we have compared the compressive properties of acellular constructs with four different filament gaps, which generated four different porosities respectively. Figure 7(*c*) compares the stress–strain curves of samples with both 90° and 60° structures. While both curves follow the same trend, the 60° structures yield higher compression modulus and yield strength.

Yield strength and compression modulus are compared and both of them decrease with the increase in porosity (see figure 7). Compression moduli were estimated based on a linear region at small and large strain regions, respectively. Yield strength is in the range of 50–100 kPa with porosity from 0.36 to 0.56, compression modulus during small strain (0–0.1) is about 25–40 kPa and during large strain (0.25–0.35) is about 80–140 kPa. Moreover, the data point for the 60° structure is above the trend line for yield strength and modulus under large strain, which indicates the triangle units enhance the soft tissue models with the same porosity (figure 7).

3.3.3. Data fitting with material models. Exponential function (4), power function (5) and the Ogden modified model (7) were used to fit the experimental data of day 0, day 1, day 3 and day 6 (figure 8). Table 1 lists coefficients for each material model and the fitting correlation coefficient of R-Sq. The power function deviates greatly from the experimental data under low strain (0–0.15) (see the zoomed-in section in figure 8(*a*)) and the three models have similar fitting states under higher strain. The exponential function and Ogden model fit better than the power function in general, as indicated by their fitting correlation coefficient of R-Sq.

4. Discussion

In this study, we employed the 3D cell-assembly method and constructed 3D soft tissue models with various configurations. Multitude experimental characterizations were conducted, and three material constitutive models were also examined for their suitability in fitting test data. From the characterization results of 3D soft tissue models, it is seen that structural configuration affects their mechanical properties. More importantly, it is seen that the mechanical properties and structural integrity decrease drastically after three days of culture time. In particular, for day 0, the compression modulus of the 3D soft tissue models was determined as 20 kPa (small strain of 0–0.1) or 60 kPa (large strain of 0.25–0.35); it decreases to 4 or 14 kPa one day later and 0.4 or 1.5 kPa three days later, respectively. The test data at day 0 and day 1 are in the same range as the results reported in the literature. For example, the Young's modulus of printed alginate scaffolds without culture conditions was determined to range from 4.5 to 7.6 kPa corresponding to 66%–35% porosity (Fedorovich *et al* 2012).

Based on our observation (figure 3(*d*)), the degradation of the gelatin material occurred during the first day under culture conditions due to the temperature change; this can be considered as a major factor for the initial decrease of mechanical properties. Accelerated alginate degradation observed in the 3D *in vitro* tissue models at the later stage may be due to cellular activities and exposure to the culture conditions. There are a number of studies on the determining factors influencing the stability of hydrogels under both *in vitro* and *in vivo* conditions (Shoichet *et al* 1996, LeRoux *et al* 1999, King *et al* 2001, Nunamaker *et al* 2007). Shoichet *et al* compared the stability of alginate and agarose under *in vitro* conditions and examined the effects of de-crosslinking and the presence of cells (Shoichet *et al* 1996). Their findings indicated that the decrease in alginate gel strength may have resulted from de-crosslinking with limited degradation effects from Calf adrenal chromaffin (CAC) cells. In the study by LeRoux *et al* (1999), it was reported that alginate gels were sensitive to a dramatic ion-induced softening effect in physiological levels of NaCl over a time period of up to seven days after gelation. Nunamaker and co-workers investigated the effects of *in situ* gelling, diffusion gelling and a poly-L-lysine (PLL) coating on the *in vivo* stability and biocompatibility of calcium alginate (Nunamaker *et al* 2007). While PLL coating increased the stability to some degree, *in situ* gelling yielded much higher stability. For the bioprinted *in vitro* soft tissue models, understanding the change of mechanical properties and structural integrity under culture conditions can provide insights to how well the tissue models mimic the *in vivo* mechanochemical microenvironment and the initial 3D environment is maintained for cells, especially during the initial stage. Modifications such as optimizing matrix

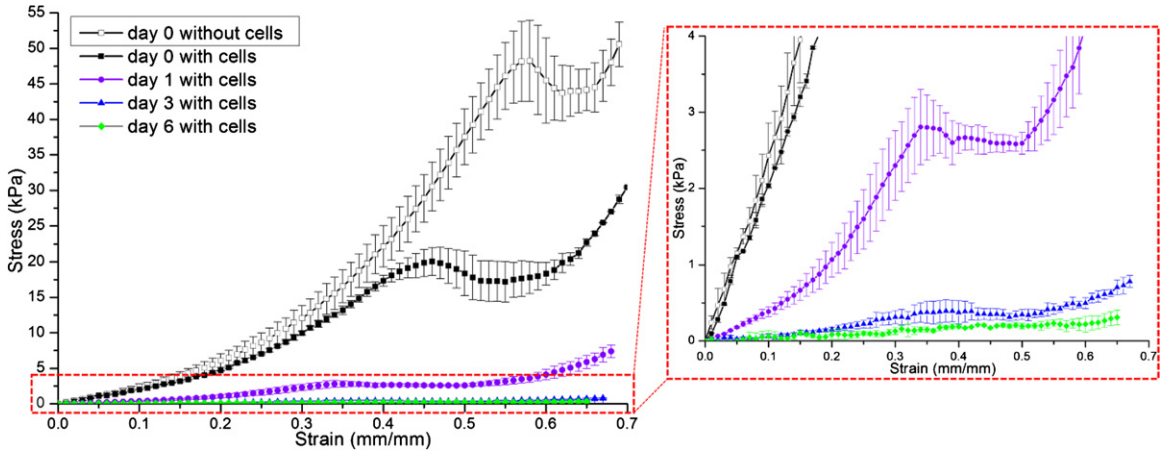

Figure 6. Stress–strain curve of *acellular constructs* at day 0 and soft tissue models cultured for different days.

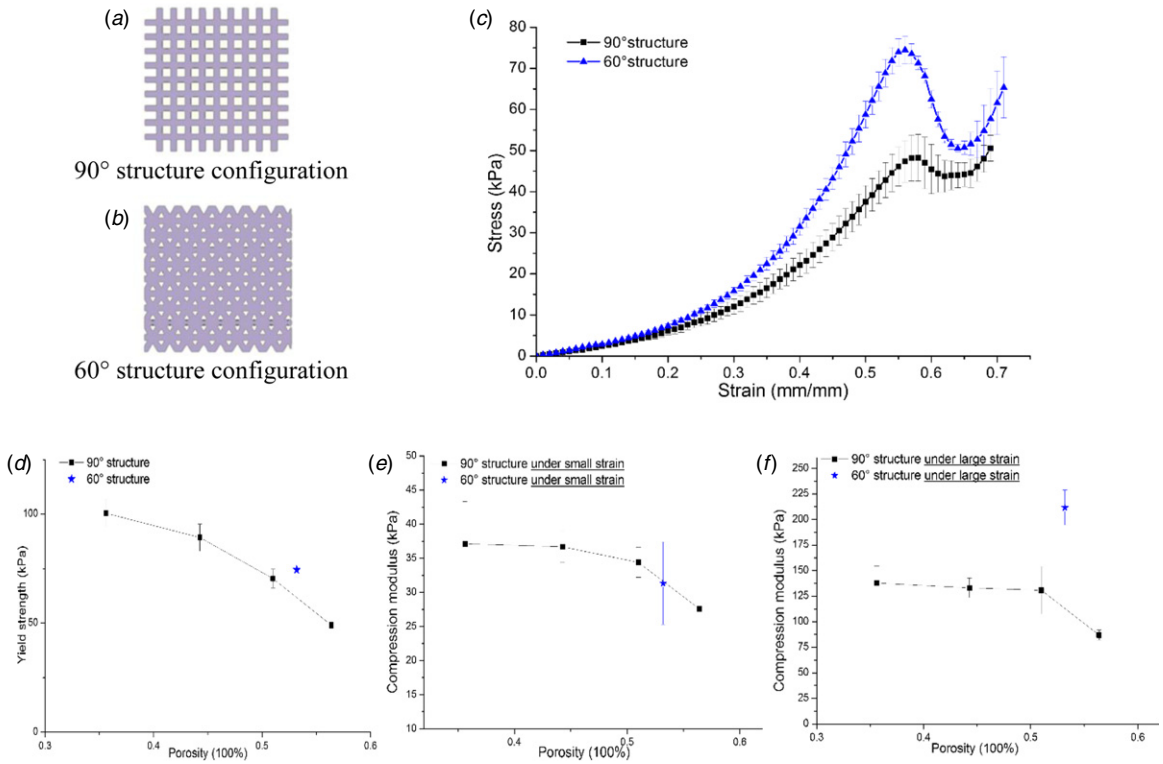

Figure 7. Two configurations: (*a*) 90° structure and (*b*) 60° structure. (*c*) Stress–strain curve of the constructs with 90° structure and 60° structure. Mechanical properties of printed acellular constructs with different structures: (*d*) the yield strength, (*e*) compression modulus under small strain (0–0.1) and (*f*) compression modulus under large strain (0.25–0.35).

Table 1. The values of fitting parameters and correlation coefficient for different models.

		0d	1d	3d	6d
Exponential func. $\sigma = A(e^{B\varepsilon} - 1)$	A	3.208 ± 0.0784	0.565 ± 0.0247	0.180 ± 0.0247	0.215 ± 0.1048
	B	4.668 ± 0.0572	5.345 ± 0.1190	3.190 ± 0.2779	1.528 ± 0.5801
	Adj. R-Sq	0.99 931	0.99 817	0.98 510	0.89 210
Power func. $\sigma = A\varepsilon^B$	A	85.53 ± 3.0916	18.685 ± 0.6891	1.719 ± 0.0915	0.540 ± 0.0671
	B	1.768 ± 0.0318	1.753 ± 0.0284	1.468 ± 0.0433	1.207 ± 0.1012
	Adj. R-Sq	0.99 517	0.99 670	0.99 670	0.89 740
Ogden model $\sigma = \mu((1+\varepsilon)^{\alpha} - (1+\varepsilon)^{-\frac{\alpha}{2}})$	μ	1.453 ± 0.0282	0.266 ± 0.0099	0.070 ± 0.0073	0.053 ± 0.0167
	α	7.478 ± 0.0628	8.287 ± 0.1385	5.794 ± 0.3294	4.076 ± 0.8415
	Adj. R-Sq	0.99 936	0.99 800	0.99 800	0.90 050

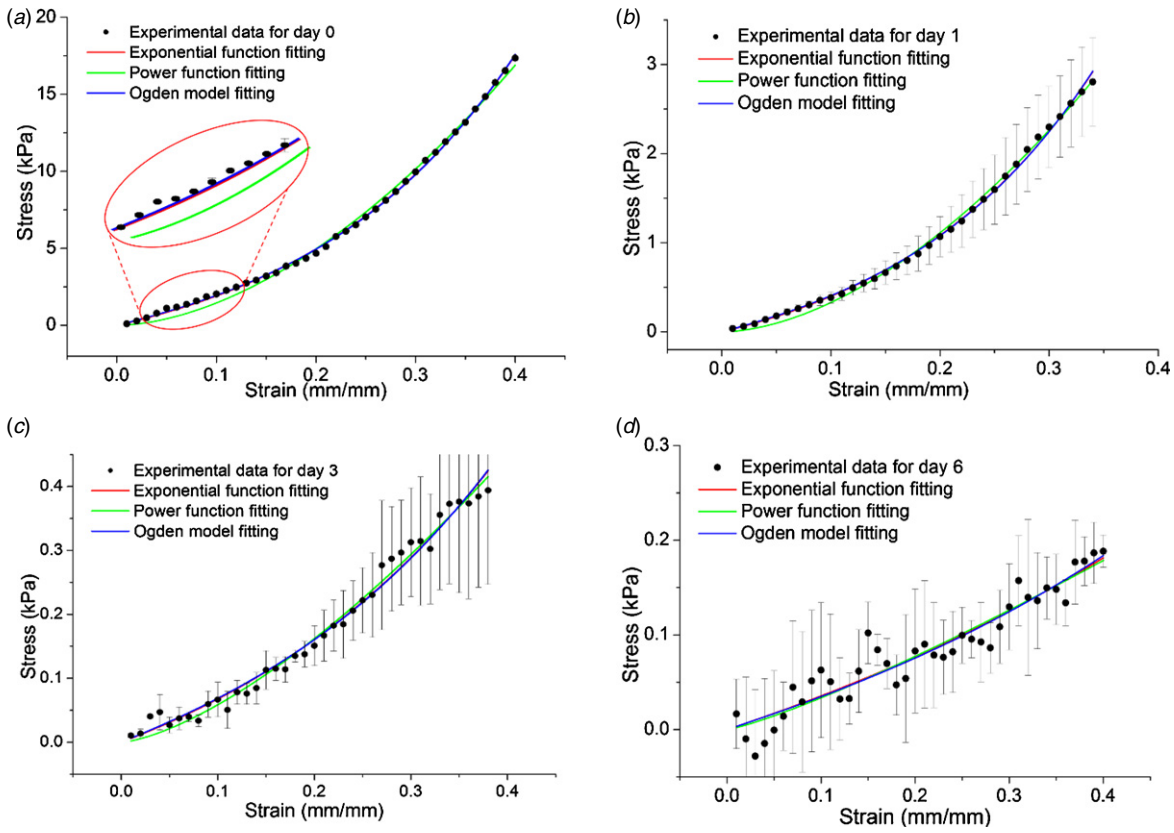

Figure 8. The fitting results of experimental data and mechanical models at (*a*) day 0, (*b*) day 1, (*c*) day 3 and (*d*) day 6.

materials and/or incorporating extra steps in culture protocol may be necessary to better control the change of mechanical properties and structural integrity under culture conditions. It was reported that the scaffolds were incubated in $CaCl_2$ once a week to prevent gel weakening (Fedorovich *et al* 2012). Currently, we are working on modifying the scaffold matrix materials via incorporating fibrin to improve the mechanical properties and structural integrity.

It is also noted that literature results on the mechanical properties obtained from the biological soft tissue extracted *in vivo* have a wide range. For instance, Hu and Desai estimated local effective elastic moduli in the range of 50–250 kPa based on the experimental data of probing liver samples (Hu and Desai 2004). Brunon *et al* reported that the elastic moduli for liver were estimated as 16.97 ± 9.9 MPa (11 samples) and 27.57 ± 22.7 MPa (16 samples) for fresh and frozen human liver capsules, respectively, and 11.67 ± 19.2 MPa (15 samples) and 7.87 ± 10.5 MPa (14 samples) for fresh and frozen porcine capsules, respectively (Brunon *et al* 2010). In order to better mimic the biological soft tissues, further development is needed to optimize matrix materials and construct the configuration of a 3D *in vitro* soft tissue model for a given cell/tissue type.

In addition, the results from biological characterization show relative low cell viability (54.72% in average) right after printing, but the cells remain active, which can be seen from the proliferation data and live/dead staining results at day 1 and day 2. It is thought that shear stresses experienced by the cells and the low temperature (∼20 min and 4 °C) during the printing process are potential key contributors to low cell viability. Current on-going effort focuses on examining the effects of process parameters and fine-turning the process to better control the resulting cell viability.

5. Conclusions

In this study, 3D cell-encapsulated hydrogel constructs with different structures were fabricated using the 3D cell-assembly technique; uniaxial compression tests were performed. Results show that the strength of the constructs decrease with increasing porosity under the same structural configuration, and configuration with angled layers (like the 60° structure) enhance the strength of printed constructs compared to a 0°/90° configuration. Test results also show a decreasing trend for both the compressive modulus and the strength of the bioprinted tissue models during the first week of culture, especially after three days of culture time. In addition, the experimental data fit well with the Ogden model and the experiential function. The characterization provides us with a foundation to further study the relation between mechanical properties, biodegradation and consequent cellular behaviours in the *in vitro* soft tissue models, and take into account combined effects in the design and fabrication of *in vitro* soft tissue models. On-going and future efforts include more in-depth investigation of matrix materials, soft tissue structure design and the fine-tuning of printing processes.

Acknowledgments

The authors acknowledge the funding supports from the National Natural Science Foundation of China through project no. 51235006, the National High Technology Research and Development Program of China (863 Program) through project no. 2012AA020506 and the Shenzhen Development and Reform Commission.

References

Atala A, Bauer S B, Soker S, Yoo J J and Retik A B 2006 Tissue-engineered autologous bladders for patients needing cystoplasty *Lancet* **367** 15–21

Awad H A, Wickham M Q, Leddy H A, Gimble J M and Guilak F 2004 Chondrogenic differentiation of adipose-derived adult stem cells in agarose, alginate, and gelatin scaffolds *Biomaterials* **25** 3211–22

Barron J A, Wu P, Ladouceur H D and Ringeisen B R 2004 Biological laser printing: a novel technique for creating heterogeneous 3-dimensional cell patterns *Biomed. Microdevices* **6** 139–47

Brunon A, Bruyere-Garnier K and Coret M 2010 Mechanical characterization of liver capsule through uniaxial quasi-static tensile tests until failure *J. Biomech.* **43** 2221–7

Ceelen K K, Oomens C, Stekelenburg A, Bader D L and Baaijens F 2009 Changes in intracellular calcium during compression of C_2C_{12} myotubes *Exp. Mech.* **49** 25–33

Chang R, Emami K, Wu H and Sun W 2010 Biofabrication of a three-dimensional liver micro-organ as an *in vitro* drug metabolism model *Biofabrication* **2** 045004

Chang R, Nam J and Sun W 2008 Direct cell writing of 3D microorgan for *in vitro* pharmacokinetic model *Tissue Eng. C Methods* **14** 157–66

De Santis R *et al* 2011 A basic approach toward the development of nanocomposite magnetic scaffolds for advanced bone tissue engineering *J. Appl. Polym. Sci.* **122** 3599–605

Derby B 2012 Printing and prototyping of tissues and scaffolds *Science* **338** 921–6

Domingos M, Chiellini F, Gloria A, Ambrosio L, Bartolo P and Chiellini E 2012 Effect of process parameters on the morphological and mechanical properties of 3D Bioextruded poly(ε-caprolactone) scaffolds *Rapid Prototyping J.* **18** 56–67

Drury J L and Mooney D J 2003 Hydrogels for tissue engineering: scaffold design variables and applications *Biomaterials* **24** 4337–51

Fedorovich N E, Schuurman W, Wijnberg H M, Prins H J, van Weeren P R, Malda J, Alblas J and Dhert W J 2012 Biofabrication of osteochondral tissue equivalents by printing topologically defined, cell-laden hydrogel scaffolds *Tissue Eng. C Methods* **18** 33–44

Fung Y 1993 *Biomechanics: Mechanical Properties of Living Tissues* (New York: Springer)

Gasser T C, Ogden R W and Holzapfel G A 2006 Hyperelastic modelling of arterial layers with distributed collagen fibre orientations *J. R. Soc. Interface* **3** 15–35

Giordano C, Albani D, Gloria A, Tunesi M, Batelli S, Russo T, Forloni G, Ambrosio L and Cigada A 2009 Multidisciplinary perspectives for Alzheimer's and Parkinson's diseases: hydrogels for protein delivery and cell-based drug delivery as therapeutic strategies *Int. J. Artif. Organs* **32** 836–50

Gloria A, Borzacchiello A, Causa F and Ambrosio L 2012a Rheological characterization of hyaluronic acid derivatives as injectable materials toward nucleus pulposus regeneration *J. Biomater. Appl.* **26** 745–59

Gloria A, Causa F, Russo T, Battista E, Della Moglie R, Zeppetelli S, De Santis R, Netti P A and Ambrosio L 2012b Three-dimensional poly(epsilon-caprolactone) bioactive scaffolds with controlled structural and surface properties *Biomacromolecules* **13** 3510–21

Hollister S J 2005 Porous scaffold design for tissue engineering *Nature Mater.* **4** 518–24

Hu T and Desai J P 2004 Characterization of soft-tissue material properties: large deformation analysis *Med. Simul.* **3078** 28–37

Humphrey J D 2003 Review paper: continuum biomechanics of soft biological tissues *Proc. R. Soc. Lond.* A **459** 3–46

Jakab K *et al* 2008 Tissue engineering by self-assembly of cells printed into topologically defined structures *Tissue Eng.* **14** 413–21

Khalil S, Nam J and Sun W 2005 Multi-nozzle deposition for construction of 3D biopolymer tissue scaffolds *Rapid Prototyping J.* **11** 9–17

Khatiwala C, Law R, Shepherd B, Dorfman S and Csete M 2012 3D Cell bioprinting for regenerative medicine research and therapies *Gene Ther. Regul.* **7** 1230004

King A, Sandler S and Andersson A 2001 The effect of host factors and capsule composition on the cellular overgrowth on implanted alginate capsules *J. Biomed. Mater. Res.* **57** 374–83

Kuo C K and Ma P X 2001 Ionically crosslinked alginate hydrogels as scaffolds for tissue engineering: part 1. Structure, gelation rate and mechanical properties *Biomaterials* **22** 511–21

Lazic T and Falanga V 2011 Bioengineered skin constructs and their use in wound healing *Plast. Reconstr. Surg.* **127** 75s–90s

Lee S H, Moon J J and West J L 2008 Three-dimensional micropatterning of bioactive hydrogels via two-photon laser scanning photolithography for guided 3D cell migration *Biomaterials* **29** 2962–8

Lee W, Debasitis J C, Lee V K, Lee J-H, Fischer K, Edminster K, Park J-K and Yoo S-S 2009 Multi-layered culture of human skin fibroblasts and keratinocytes through three-dimensional freeform fabrication *Biomaterials* **30** 1587–95

LeRoux M A, Guilak F and Setton L A 1999 Compressive and shear properties of alginate gel: effects of sodium ions and alginate concentration *J. Biomed. Mater. Res.* **47** 46–53

Liu H X, Li S J and Yan Y N 2011 Cell direct assembly technology adopting hybrid of gelatin-based hydrogels *Manuf. Process. Technol.* **189–193** 2986–92

Liu V A and Bhatia S N 2002 Three-dimensional photopatterning of hydrogels containing living cells *Biomed. Microdevices* **4** 257–66

Lutolf M P and Hubbell J A 2005 Synthetic biomaterials as instructive extracellular microenvironments for morphogenesis in tissue engineering *Nature Biotechnol.* **23** 47–55

Masouros S D, Parker K H, Hill A M, Amis A A, Bull A M J and Yoganandan N 2009 Testing and modelling of soft connective tissues of joints: a review *J. Strain Anal. Eng. Des.* **44** 305–18

McAllister T N *et al* 2009 Effectiveness of haemodialysis access with an autologous tissue-engineered vascular graft: a multicentre cohort study *Lancet* **373** 1440–6

Mironov V, Boland T, Trusk T, Forgacs G and Markwald R R 2003 Organ printing: computer-aided jet-based 3D tissue engineering *Trends Biotechnol.* **21** 157–61

Nekouzadeh A, Pryse K M, Elson E L and Genin G M 2007 A simplified approach to quasi-linear viscoelastic modeling *J. Biomech.* **40** 3070–8

Norotte C, Marga F S, Niklason L E and Forgacs G 2009 Scaffold-free vascular tissue engineering using bioprinting *Biomaterials* **30** 5910–7

Nunamaker E A, Purcell E K and Kipke D R 2007 *In vivo* stability and biocompatibility of implanted calcium alginate disks *J. Biomed. Mater. Res.* A **83** 1128–37

Pai S and Ledoux W R 2011 The quasi-linear viscoelastic properties of diabetic and non-diabetic plantar soft tissue *Ann. Biomed. Eng.* **39** 1517–27

Rehfeldt F, Engler A J, Eckhardt A, Ahmed F and Discher D E 2007 Cell responses to the mechanochemical

microenvironment—implications for regenerative medicine and drug delivery *Adv. Drug Deliv. Rev.* **59** 1329–39
Russo T *et al* 2010 Poly(ε-caprolactone) reinforced with sol-gel synthesized organic-inorganic hybrid fillers as composite substrates for tissue engineering *J. Appl. Biomater. Biomech.* **8** 146–52 PMID: 21337305
Shoichet M S, Li R H, White M L and Winn S R 1996 Stability of hydrogels used in cell encapsulation: an *in vitro* comparison of alginate and agarose *Biotechnol. Bioeng.* **50** 374–81
Subramanian A, Krishnan U M and Sethuraman S 2009 Development of biomaterial scaffold for nerve tissue engineering: biomaterial mediated neural regeneration *J. Biomed. Sci.* **16** 108
Tissue Eng 2007 Advancing tissue science and engineering: a foundation for the future. A multi-agency strategic plan *Tissue Eng.* **13** 2825–6
Umale S, Chatelin S, Bourdet N, Deck C, Diana M, Dhumane P, Soler L, Marescaux J and Willinger R 2011 Experimental *in vitro* mechanical characterization of porcine Glisson's capsule and hepatic veins *J. Biomech.* **44** 1678–83
Vunjak-Novakovic G, Martin I, Obradovic B, Treppo S, Grodzinsky A J, Langer R and Freed L E 1999 Bioreactor cultivation conditions modulate the composition and mechanical properties of tissue-engineered cartilage *J. Orthop. Res.* **17** 130–8
Yan K C, Nair K and Sun W 2010 Three dimensional multi-scale modelling and analysis of cell damage in cell-encapsulated alginate constructs *J. Biomech.* **43** 1031–8
Yan Y *et al* 2005 Fabrication of viable tissue-engineered constructs with 3D cell-assembly technique *Biomaterials* **26** 5864–71
Yang S F, Leong K F, Du Z H and Chua C K 2001 The design of scaffolds for use in tissue engineering: part 1. Traditional factors *Tissue Eng.* **7** 679–89